Preliminary Report on the 29 July 2008 Mw 5.4 Chino Hills, Eastern Los Angeles Basin, California, Earthquake Sequence

Egill Hauksson,[1] Karen Felzer,[2] Doug Given,[2] Michal Giveon,[1] Susan Hough,[2] Kate Hutton,[1] Hiroo Kanamori,[1] Volkan Sevilgen,[2] Shengji Wei,[1] and Alan Yong[2]

INTRODUCTION

The 29 July 2008 *Mw* 5.4 Chino Hills earthquake was the largest event to occur within the greater Los Angeles metropolitan region since the *Mw* 6.7 1994 Northridge earthquake. The earthquake was widely felt in a metropolitan region with a population of more than 10 million people and was recorded by hundreds of broadband and strong-motion instruments. In this report we present preliminary analysis of the event and discuss its significance within the seismotectonic framework of the northern Los Angeles basin as revealed by previous moderate earthquakes.

The Chino Hills mainshock-aftershock sequence began at a depth of about 15 km in the east Los Angeles area at 11:42 AM (PST) (Figure 1). The epicenter is between two mapped faults: the Whittier fault to the west and the Chino Hills fault to the east. The focal mechanism indicates a mixture of strike-slip and thrust faulting on a west-southwest or a west-northwest striking nodal plane. The mainshock was followed by only two aftershocks with **M** >3; **M** 3.8 at 11:52 AM (PST) and **M** 3.6 at 13:40 (PST). In the first two hours, 37 smaller aftershocks were also recorded in the magnitude range of 1.3 to 2.8. By 14 August the Southern California Seismic Network (SCSN), a joint project of the California Institute of Technology (Caltech) and the U.S. Geological Survey (USGS) had recorded ~ 150 aftershocks of **M** ≥ 1.0. The mainshock was not preceded by foreshock activity.

During the 2008 Chino Hills sequence, the SCSN automatically processed real-time waveform data from 370 stations across southern California. The first location and *ML* magnitude estimate of 5.6 were released ~ 80 s after the origin time. An updated location and final *ML* 5.8 were released after ~ 140 s. The automatic moment tensor and the *Mw* estimate of 5.4 were available ~ 10 minutes following the origin time. These SCSN rapid notifications were posted on the Web, and data were made available via http://www.data.scec.org and http://earthquake.usgs.gov.

1. California Institute of Technology
2. U.S. Geological Survey

The Chino Hills sequence was widely felt across southern California, although damage was minimal. Relatively strong shaking was recorded to the north in the Diamond Bar area and to the northwest in the eastern Los Angeles basin, as demonstrated in the ShakeMap (Wald, Quitoriano, Dengler *et al.* 1999) and actual strong-motion records, which were made available via http://www.strongmotioncenter.org. The initial ShakeMap was available 12 minutes after the origin time, in part due to a computer malfunction, but normal production time is about five minutes; six updates of the ShakeMap followed during the next hour as more data arrived from near real-time stations (Figure 2). The final map included amplitudes from 526 California Integrated Seismic Network (CISN) stations. Over 40,000 people filled out the Internet "Did You Feel It?" form to describe the effects of the earthquake at locations throughout southern California.

Five other moderate-sized mainshock-aftershock sequences have occurred in the general vicinity of the Chino Hills earthquake since 1987. The largest event was the Whittier Narrows earthquake of 1 October 1987, which was located about 30 km west-northwest and had a magnitude of 5.9. It caused three direct fatalities and over $358 million in damage. The Whittier Narrows earthquake resulted from thrust faulting on the Puente Hills thrust (Shaw and Shearer 1999). The other four earthquakes were the **M** 4.6 1989 Montebello, **M** 5.0 1988 Pasadena, **M** 5.2 1990 Upland, and **M** 5.8 1991 Sierra Madre. The 1989 Montebello earthquake was caused by thrust faulting, similar to the Whittier Narrows mainshock (Hauksson 1990). Both the Pasadena and the Upland earthquakes exhibited west-southwest left lateral strike-slip faulting while the Sierra Madre earthquake exhibited thrust faulting (Jones *et al.* 1990; Hauksson and Jones 1991; Hauksson 1994; Shearer 1997; Astiz *et al.* 2000). Thus the crustal deformation associated with the 2008 Chino Hills earthquake is similar to deformation associated with the previous events.

MAINSHOCK MOMENT TENSOR

A real-time SCSN moment tensor solution (Clinton *et al.* 2006), which was derived using an automated analysis of waveforms from six stations and the inversion method of Dreger and Helmberger (1993), revealed a strike of 291°, a dip of 59°, and

doi: 10.1785/gssrl.79.6.855

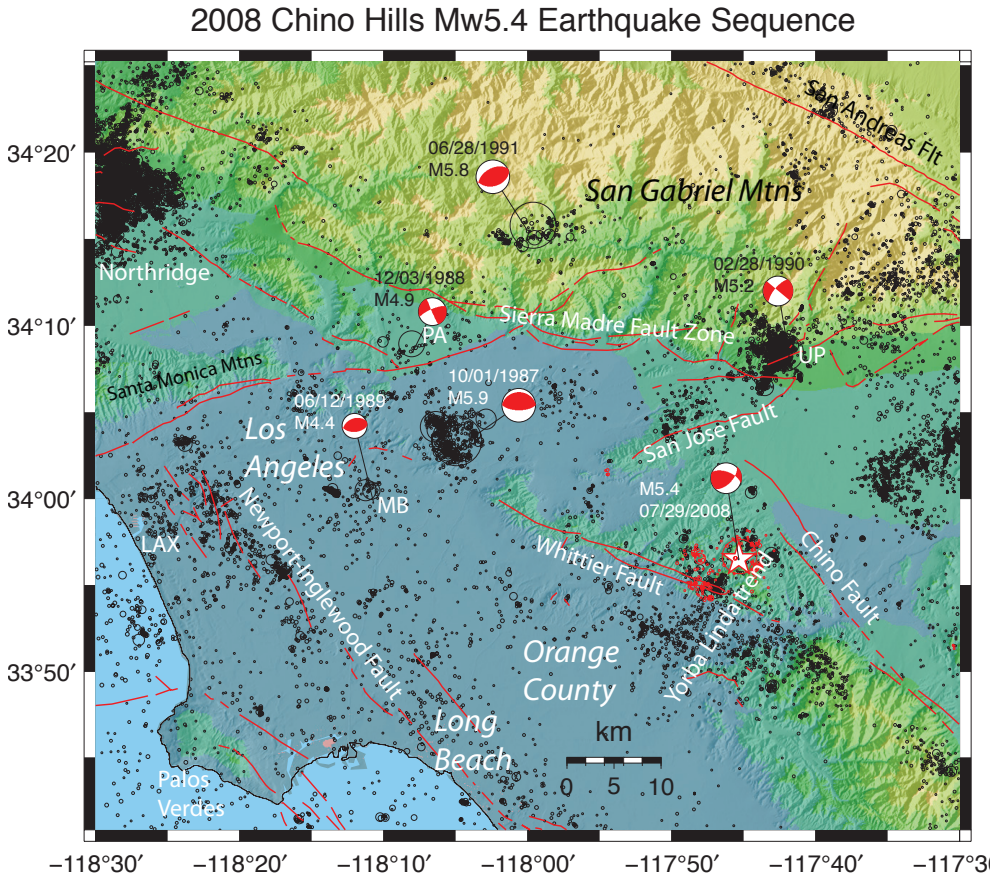

▲ **Figure 1.** Map of (1981 to 2005) seismicity recorded by the SCSN and some recent sequences in the Los Angeles basin, including lower hemisphere focal mechanisms of the moderate-sized mainshocks. The 2008 Chino Hills mainshock is shown as a red star and the aftershocks as red circles. LAX—Los Angeles Airport, MB—Montebello; PA—Pasadena; UP—Upland; WN—Whittier Narrows.

a rake of 142°. The double-couple solution was also determined using the "cut-and-paste" technique (Zhao and Helmberger 1994; Zhu and Helmberger 1996). In the "cut-and-paste," we analyzed the broadband waveforms of regional seismograms from 22 stations with epicentral distances between 100 and 200 km and maximum azimuth gap of 32° (Figure 3A). The errors in the strike, dip, and rake of the focal mechanism are about ±3°, ±6°, and ±15°, respectively.

The Green's functions were generated from the FK technique (Zhu and Rivera 2002) and were based on a 1-D southern California velocity model (Zhao and Helmberger 1994). A source depth of 15 km and *Mw* 5.4 correspond to minimum error between the real and synthetic waveforms (Figure 3B). The high cross-correlation coefficients (Figure 3C) confirm the similarity of the synthetics with the data, both for the *Pnl* waves and the surface waves. Because the "cut and paste" allows time shifts between portions of seismograms and synthetics, the results of this method are relatively insensitive to minor changes in the velocity model and to possible lateral crustal variations (Zhu and Helmberger 1996).

The global centroid moment tensor (CMT) solution (http://www.globalcmt.org/CMTsearch.html) for this event yields a best double-couple with the nodal planes (strike/dip/rake) 43°/62°/31°, 297°/63°/149° with *Mw* = 5.4. The *W* phase inversion (Kanamori and Rivera, 2008), using 18 broadband SCSN stations with a pass-band of 50 to 150 s, yields a similar mechanism and *Mw* ((strike/dip/rake) 51°/38°/32°, 294°/71°/123°, *Mw* = 5.4). The main difference between the global CMT solution and the WP inversion is in the dip angle of the southeast-dipping plane. These solutions represent the long-period characteristics of the source, and the good agreement between the regional, global, and long-period solutions suggests that the source was associated with no significant anomalous long-period (up to 100 s) deformation.

RELOCATIONS AND FOCAL MECHANISMS

We relocated the mainshock and aftershocks, using a 3-D velocity model and HypoDD (Waldhauser and Ellsworth 2000). The relocations reveal minimal clustering around either mainshock nodal plane (Figure 4). In addition, the aftershocks occurred in a limited depth range from 13 to 16 km and form a tight subhorizontal distribution. It is thus not easy to determine from the spatial aftershock patterns which of the two steeply dipping nodal planes ruptured in the mainshock. Further, the mainshock is located at a depth of 15 km, midway between the Whittier and Chino faults, and because of its large focal depth, projecting the nodal planes up to dipping surface faults is difficult at best.

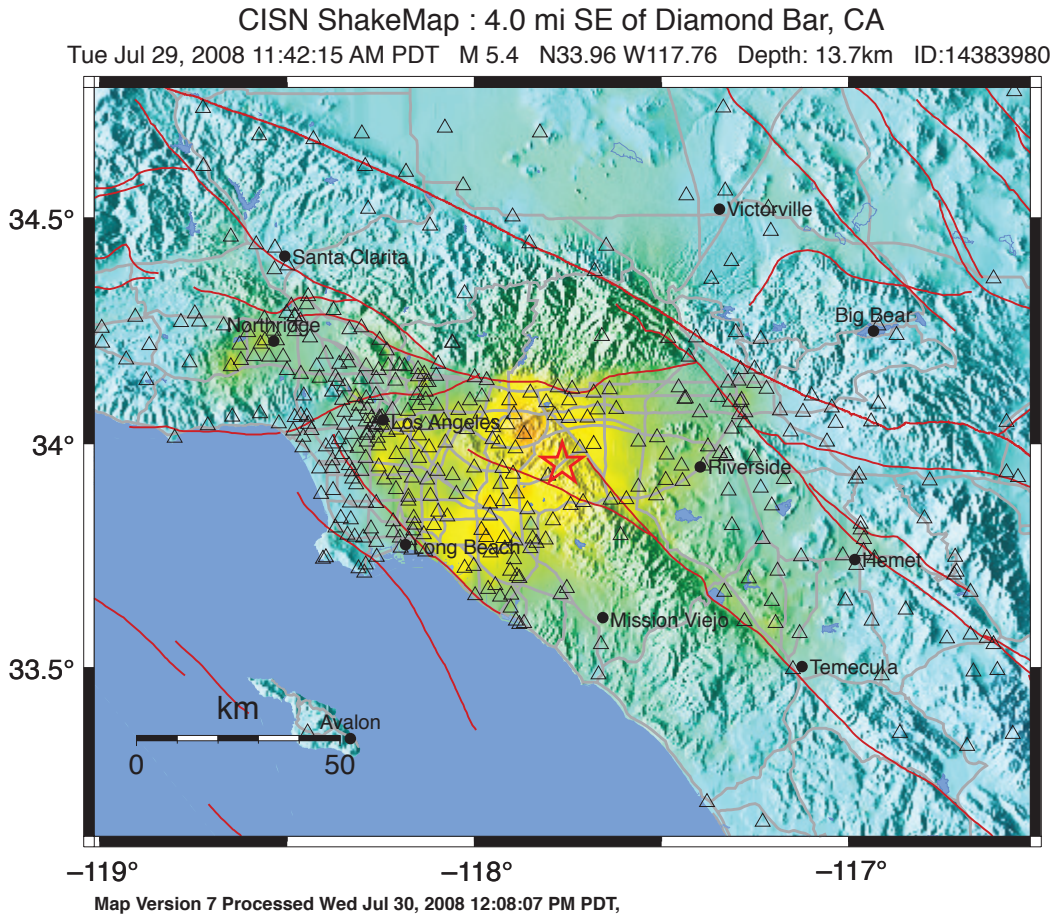

PERCEIVED SHAKING	Not felt	Weak	Light	Moderate	Strong	Very strong	Severe	Violent	Extreme
POTENTIAL DAMAGE	none	none	none	Very light	Light	Moderate	Moderate/Heavy	Heavy	Very Heavy
PEAK ACC.(%g)	*<.17*	*.17–14*	*1.4–39*	*3.9–92*	*9.2–18*	18–34	34–65	65–124	>124
PEAK VEL.(cm/s)	<0.1	0.1–1.1	1.1–34	3.4–8.1	*8.1–16*	*16–31*	*31–60*	*60–116*	*>116*
INSTRUMENTAL INTENSITY	I	II–III	IV	V	VI	VII	VIII	IX	X+

▲ **Figure 2.** The SCSN/CISN ShakeMap map of Modified Mercalli Intensities for the *Mw* 5.4 Chino Hills mainshock: http://earthquake.usgs.gov/eqcenter/shakemap/list.php?y=2008&n=sc (Wald, Quitoriano, Dengler *et al.* 1999). Triangles are seismic stations that reported strong ground motion. Mapped fault traces are from Jennings (1994).

In map view, the aftershocks scatter from the Chino fault in the northeast across the mapped trace of the Whittier fault and coincide with the Yorba Linda trend to the southwest, as defined by Hauksson (1990). Almost no aftershocks occurred in the immediate vicinity of the mainshock or within a radius of 1.5 km. The seismicity within the Yorba Linda trend extends from a few kilometers depth down to 16-km depth. If the south-dipping east-northeast-trending nodal plane was the fault plane, it would intersect the surface near the San Jose fault to the north. However, the San Jose fault could not be the causative fault, because it dips steeply to the north, and the Chino Hills sequence is located ~15 km distance to the south. The 1990 **M** 5.2 Upland earthquake was associated with the San Jose fault but at a shallower depth of 5 to 10 km (Hauksson and Jones 1991).

The northeast-dipping nodal plane of the mainshock has a strike very similar to that of the Whittier fault. However, associating the mainshock with the Whittier fault becomes difficult because the fault dip is uncertain, and the aftershock locations do not provide additional constraints. The Whittier fault has a steep dip of ~80° in the near-surface but the dip gradually shallows out to ~60° when it reaches depths of 5 km or greater (Bjorklund and Burke 2002; Bjorklund *et al.* 2002). Thus some of the aftershocks are clearly located in the footwall block of the Whittier fault, including the largest off-fault aftershock cluster. Both the **M** 3.6 and **M** 3.8 aftershocks also formed their own aftershock clusters. We used the method of Hardebeck and Shearer (2002) to determine the first-motion focal mechanisms for the **M** 3 aftershocks. Their focal mechanisms exhibited strike-slip motion on northwest- or northeast-striking planes, while the focal mechanisms of the smaller aftershocks exhibit a heterogeneous mixture of strike-slip and thrust faulting, with some minor normal faulting.

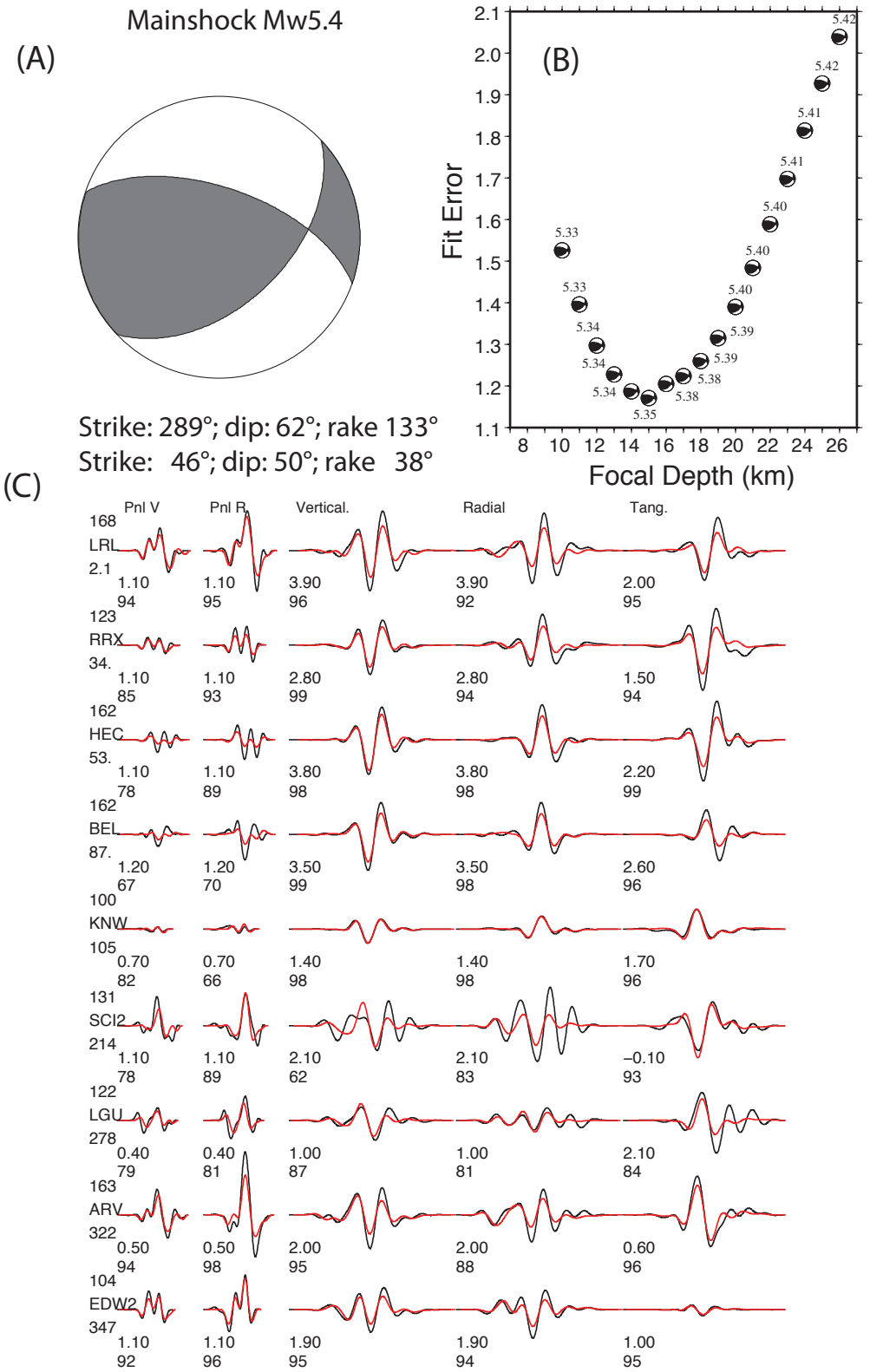

▲ **Figure 3.** (A) The focal mechanism of the mainshock "cut-and-paste" source estimation technique. (B) The misfit variations represented by the fit-error as a function of focal depth. The number above each focal mechanism image is the corresponding *Mw*. (C) Selected regional broadband displacement seismograms of the Chino Hill event. The synthetics are plotted in red and the data in black. The numbers above the station names are the epicenter distances in kilometers and the numbers below are the azimuths. The first number below each seismogram is the time shift between data and synthetics (positive means synthetic is faster than the data, or synthetic has to shift back to fit the data) and the second number is the cross-correlation coefficient as a percentage.

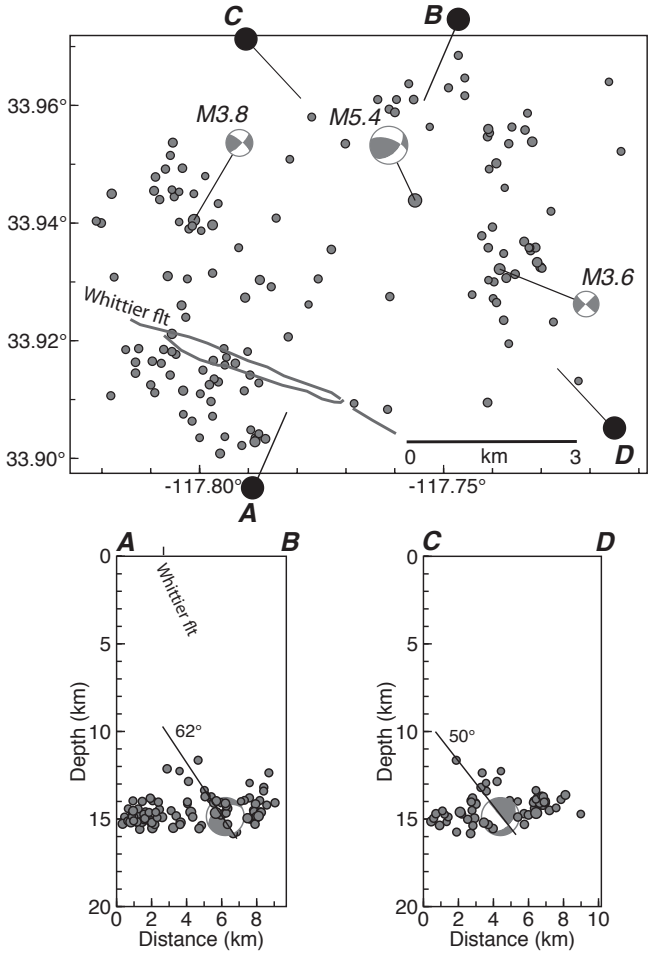

▲ **Figure 4.** Map and ±3 km-wide cross-sections of the details of the seismicity. The symbol size is scaled linearly with magnitude. The first-motion focal mechanisms for the **M** 3.6 and **M** 3.8 aftershocks are also shown.

MAINSHOCK STRESS DROP

The 2008 Chino Hills earthquake excited impulsive *S* waves that were recorded at many close-in stations. The pulse width, τ, is approximately 1 s. Here τ is measured from the *S*-wave pulses observed on the horizontal component records at nine SCSN non-nodal stations (BRE, PDU, WLT, CHN, RUS, LLS, FUL, DLA, and PSR) and eight strong-motion records compiled at the Center for Engineering Strong Motion Data. Although the pulse widths of *P* waves are equally narrow, we did not measure them because *P* waves are relatively small at close-in stations for this event. When plotted on a τ vs. M_0 diagram (Figure 5), the data point for this event falls on the trend defined by several Los Angeles basin earthquakes, such as the 1991 Sierra Madre, the 1988 Pasadena, and the 1989 Montebello earthquakes, which yielded the smallest pulse width for a given magnitude (dashed line in Figure 5). The pulse width for the Chino Hills earthquake is also close to the lower bound of τ of the τ vs. M_0 data set for eastern North America, western North America, and other continental interiors compiled by Somerville *et al.* (1987). Since attenuation will broaden the pulse width, the values measured

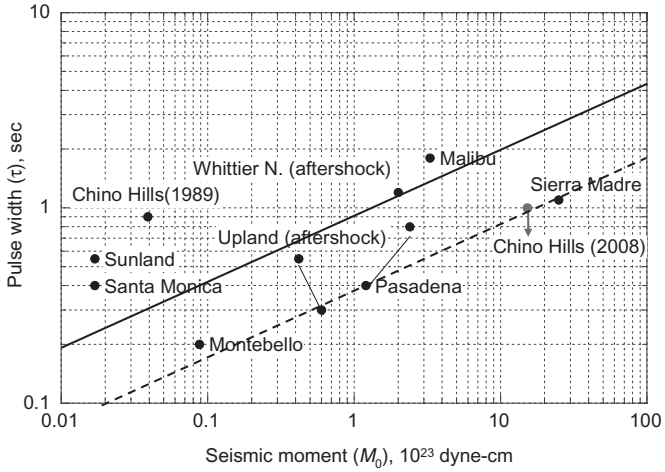

▲ **Figure 5.** Pulse widths of LA basin earthquakes adapted from Kanamori *et al.* (1993). The solid sloping line is the relationship for a global data set (Kikuchi, written communication 2001; Kanamori and Brodsky 2004).

from seismograms should be regarded as the upper bound, and the actual pulse width could be even shorter. In general, a small pulse width implies a small source dimension, which in turn implies a large stress drop, $\Delta\sigma$. The solid line in Figure 5 is the relationship for a global data set (M. Kikuchi, written communication 2001; Kanamori and Brodsky 2004). This trend is almost identical to the relationship used by the Harvard and the global CMT groups and is given by $\tau = 2.10 \times 10^{-8} M_0^{1/3}$ (τ in s and M_0 in dyne × cm). The pulse width of the Chino Hills earthquake is about 2.4 times smaller than what the global relationship predicts. Since the commonly used scaling relation gives $\Delta\sigma \propto \tau^{-3}$, the data plotted in Figure 5 would suggest that $\Delta\sigma$ of the Chino Hills earthquake is 2.4^3 (~14) times larger than the global average of large earthquakes. The empirical relation given by Cohn *et al.* (1982), $\Delta\sigma = M_0\tau^{-3}/10^{15.73}$ ($\Delta\sigma$ in MP, M_0 in N-m), leads to $\Delta\sigma \sim 30$ MP for $\tau = 1$ s. However, since $\Delta\sigma$ depends on other factors such as the rupture speed and geometry, its exact value is subject to some uncertainty, but the very short pulse width of the Chino Hills earthquake suggests that it is most likely a high-stress drop event.

Bent and Helmberger (1989) estimated the stress drop of the 1987 Whittier Narrows earthquake (*Mw* = 5.9) to be about 75 MP. Dreger and Helmberger (1991a, 1991b) estimated the stress drops of the 1990 Upland earthquake (*Mw* = 5.5) and the 1991 Sierra Madre earthquake (*Mw* = 5.8) to be 27 and 46 MP, respectively. However, these estimates depend on the assumption of the rupture dimension. Judging from the duration of the source discussed in these papers, these events would probably plot close to the dashed line of the τ vs. M_0 diagram (Figure 5). Thus, considering the uncertainties in the stress-drop estimates, the 2008 Chino Hills, the 1987 Whittier Narrows, the 1990 Upland, and the 1991 Sierra Madre earthquakes all seem to belong to a group of high stress-drop events. Our stress-drop results also agree with Shearer *et al.* (2006), who analyzed a large southern California data set and concluded that the range of stress drop for southern California is from 0.2 to 20 MP.

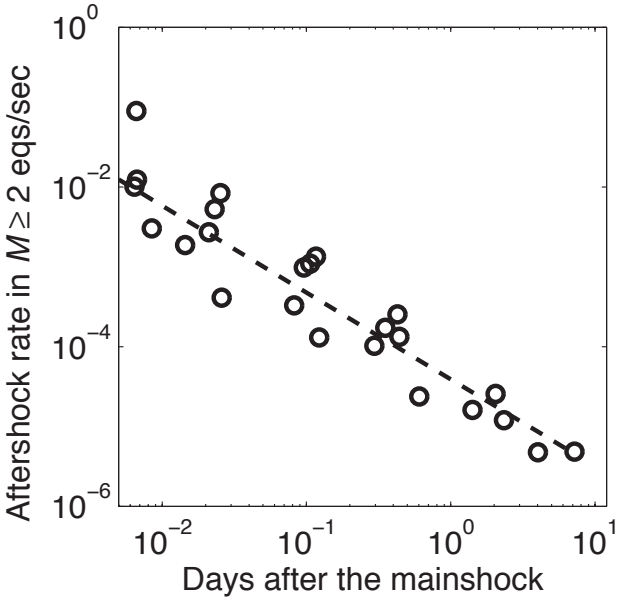

▲ **Figure 6.** Aftershock rate in terms of **M** ≥ 2 aftershocks per second as a function of time for the first ten days after the Chino Hills mainshock. Aftershock rate is solved from the time separation between successive aftershocks using the nearest neighbor method. The dashed line is the best fit Omori's law with parameters $p = 1.09$ and $K = 3.4$ where K is given in terms of **M** ≥ 2 aftershocks per day.

AFTERSHOCK STATISTICS

As of August 8, 2008, the aftershock sequence of the Chino Hills earthquake was decaying in time in accordance with the classic modified Omori law ($R(t) = K(t + c)^{-p}$) (Utsu 1961) where $R(t)$ is earthquake rate, t is time since the mainshock, and c and p are constants (Figure 6). The value of c is very small, typically difficult to determine, and unimportant after the immediate post-mainshock period. Hence we focus here on the values of K and p. As of August 8, 2008, the best fitting p value was 1.09, with a 98% confidence range from 0.91 to 1.36, and the best fitting K value was 3.4, with a 98% confidence range from 2.3 to 5.2, where K is measured in terms of **M** ≥ 2 aftershocks/day. This p value is very close to the California state average of 1.08 (Reasenberg and Jones 1989), but the K value is about 20% of the state average for an earthquake of this size (Felzer *et al.* 2003), indicating a low overall rate. As of August 8, only 26 **M** ≥ 2 aftershocks had been recorded.

Extrapolation of the current decay parameters indicate that if current trends continue, one to two **M** ≥ 2 aftershocks may be expected during the month of September 2008 and two to three **M** ≥ 2 aftershocks may be expected for the entire year of 2009. The region of the Chino Hills earthquake had been moderately active in the past, and so we inspected other local aftershock sequences to see if the low aftershock rates might have been anticipated. Using the region 33.68° to 34.24°N and −117.93° to −117.61°W and the time period 1 January 1984–30 June 2008, we identified 213 **M** ≥ 2 potential mainshocks that were reasonably isolated (at least 20 days after or five fault lengths away from larger earthquakes). These mainshocks produced **M** ≥ 2 aftershocks (defined as earthquakes occurring within 10 days and five fault lengths) at a rate of 84% of the state average, with 98% confidence intervals from 65% to 108%. Thus previous sequences had somewhat low productivity but not nearly as low as that of the Chino Hills sequence. The magnitude-frequency statistics of the Chino Hills sequence were normal, agreeing well with the Gutenberg-Richter magnitude frequency distribution (Gutenberg and Richter 1944) with a b-value of 1.0.

REMOTELY TRIGGERED EARTHQUAKES

Recent studies (*e.g.*, Hough 2005; Felzer and Brodsky 2006) have concluded that aftershock/triggered earthquake sequences following small and moderate mainshocks extend to distances of many fault lengths. To explore the spatial distribution of the aftershock sequence of the Chino Hills earthquake, we use the β-statistic to quantify the seismicity rate change at close and regional distances (*e.g.*, Matthews and Reasenberg 1988). The β-statistic, or simply β, is defined as

$$\beta = \frac{N_a - N_e}{\sqrt{u}} \quad (1)$$

where N_a is the actual number of events in a grid cell, N_e is the number expected based on the number of earthquakes before the mainshock, and u is the variance assuming a Poissonian distribution. The β-statistic can be plagued by artifacts; for example, decaying aftershock sequences in a given area will produce a negative β-statistic that is unrelated to a mainshock. It is also not necessarily safe to assume that background seismicity follows a Poissonian distribution. However, the β-statistic provides a simple measure of seismicity rate change relative to a background rate.

To further explore the seismicity rate change away from the immediate epicentral region we average the results azimuthally to obtain $\beta(r)$ (Figure 7A). We note that, as introduced by Matthews and Reasenberg (1988), N_e represents a probability density function with equal probability over a ±0.5 range bracketing whole numbers. Because the expected number of earthquakes cannot be negative, if there are no events in a pre-event window, N_e is set to 0.25. Thus if there are no events in a grid cell in the post-mainshock window ($N_a = 0$), β is not identically zero, but rather slightly negative, in this case approximately −0.7. To calculate $\beta(r)$ we therefore include only those grid cells for which there is a seismicity change. One cannot ascribe any statistical significance to the very weakly positive β values between 10 and 50 km (Figure 7B). However, previous results considering β-statistics averaged over large numbers of earthquakes suggest the small increase in seismicity over this distance range might reflect an extended aftershock zone (Hough 2005; Felzer and Brodsky 2006).

STATIC STRESS CHANGE

We calculate the static Coulomb stress imparted by the Chino Hills earthquake to its aftershocks and to nearby portions of the

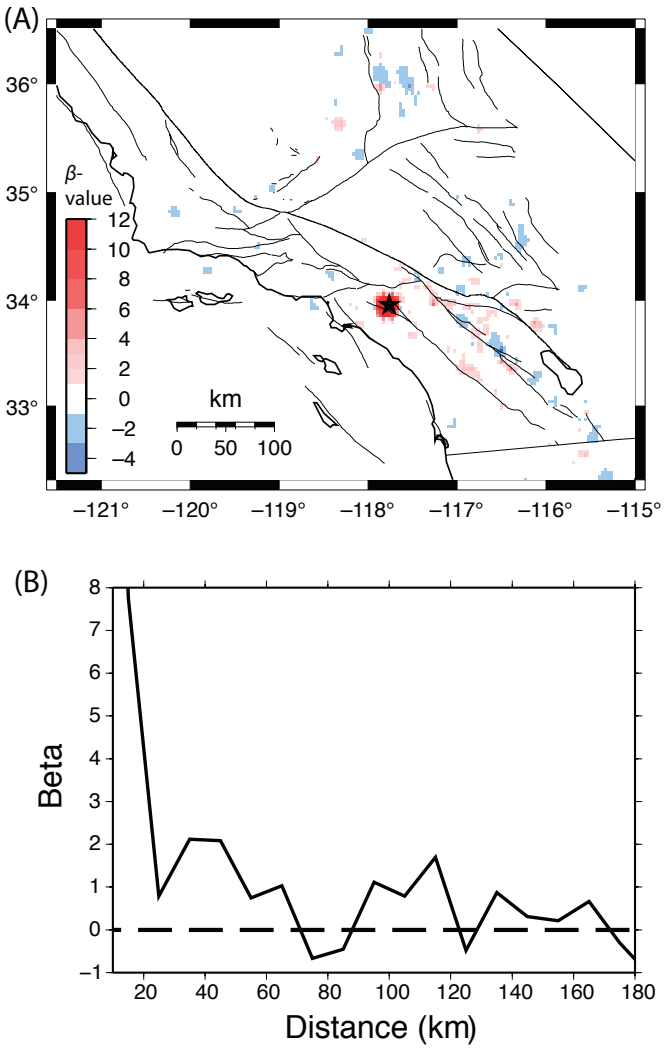

▲ **Figure 7.** (A) Map of Beta statistics. (B) Beta versus distance showing only small variations.

Whittier and Chino faults, following Lin and Stein (2004) and Toda *et al.* (2005). We use both mainshock nodal planes as candidate sources in Figures 8A–B, in each case adopting the same strike, dip, and rake for the source and receiver faults. We note that nodal plane 1 resembles the strike, rake, and location of the Whittier fault, and nodal plane 2 would reach the surface near the San Jose fault. There are more aftershocks aligned with nodal plane 1 (Figure 4, section AB) than with nodal plane 2 (Figure 4, section CD), and so perhaps the nodal plane 1 is more likely the source. We assume a 300-bar (30 MPa) mainshock shear stress drop, a friction coefficient on receiver faults of 0.4, Poisson's ratio of 0.25, and a 3.1×10^{11} dyne-cm^2 shear modulus. For the map view plots, we calculate the maximum Coulomb stress change over the depth range of the aftershocks, 14–16 km.

Regardless of the source nodal plane, the calculated lobes of increased Coulomb stress appear consistent with the distribution of aftershocks (Figures 8A–B). In cross-section (Figures 8C–D), the majority of aftershocks are seen to lie in regions of calculated Coulomb stress increase, and few aftershocks occur in the lobes of stress decrease. We note that the two aftershocks with focal mechanisms in Figure 4 display vertical strike-slip mechanisms, which differ from the receiver faults used here. The stress increase lobes for such receiver faults are consistent with the aftershock distribution for the nodal plane 2 source.

We resolve the Coulomb stress changes on the projected surfaces of the Whittier and Chino faults in Figures 8E–F, under the assumption that they are right lateral-reverse faults (Bjorklund and Burke 2002, Bjorklund *et al.* 2002; Ludington *et al.* 2007). We used a rake of 133°, the same as nodal plane 1. We used a dip of 75°; gentler dips would place the Chino Hills earthquake outside the uplifted wedge between the faults, which we regard as unlikely. For the nodal plane 1 and nodal plane 2 sources (Figures 8 E–F), the area of the Whittier fault sustaining a Coulomb stress increase is considerably larger than the area with a stress decrease; the median stress change is +0.15 bars (0.015 MPa) over the 15 × 20 km (length × width) fault patch closest to the Chino Hills source. For the Chino fault the changes are more balanced and the median stress change is +0.08 bars (0.008 MPa). Although few of the Chino Hills aftershocks appear to coincide with these faults, the aftershocks occurring near the Whittier fault lie near the patches with the greatest calculated stress increase.

DISTRIBUTION OF INTENSITIES

The Chino Hills event was widely felt throughout the greater Los Angeles region; as of 12 August 2008, more than 40,000 people filled out the Community Internet Intensity Map (CIIM), also known as the "Did You Feel It?" questionnaire (Figure 9). These responses were used to determine Modified Mercalli Intensity (MMI) values for 802 ZIP Codes (see Wald, Quitoriano, Heaton *et al.* 1999; also http://pasadena.wr.usgs.gov/shake/ca/). Because of the dense population of much of the greater Los Angeles region, intensity values averaged within ZIP Codes provide good spatial correlation to the location of the actual reporting sites (Figure 10A). We use the averages within ZIP Codes in our subsequent analysis. Our data set includes CIIM results collected as of 12 August 2008, a total of 40,677 individual questionnaires.

The averaged MMI values are first fit by a standard functional form,

$$MMI = A - br - c\log(r)\,. \qquad (2)$$

When fitting Equation 2 using a least-squares approach, the distribution of average intensities clusters closely around the curve (Figure 10B), corroborating the conclusion that CIIM intensities provide a consistent measure of earthquake ground motions (*e.g.*, Atkinson and Wald 2006).

A further indication of the stability of CIIM intensities is the generally good correspondence between the CIIM distribution and the CISN ShakeMap, which is based on peak amplitudes from instrumental recordings (see http://earthquake.usgs.gov/shakemap/; Figure 2). The ShakeMap does, however, reveal somewhat higher intensities to the northwest and southwest of the epicenter than the reported CIIM intensities. That is, at

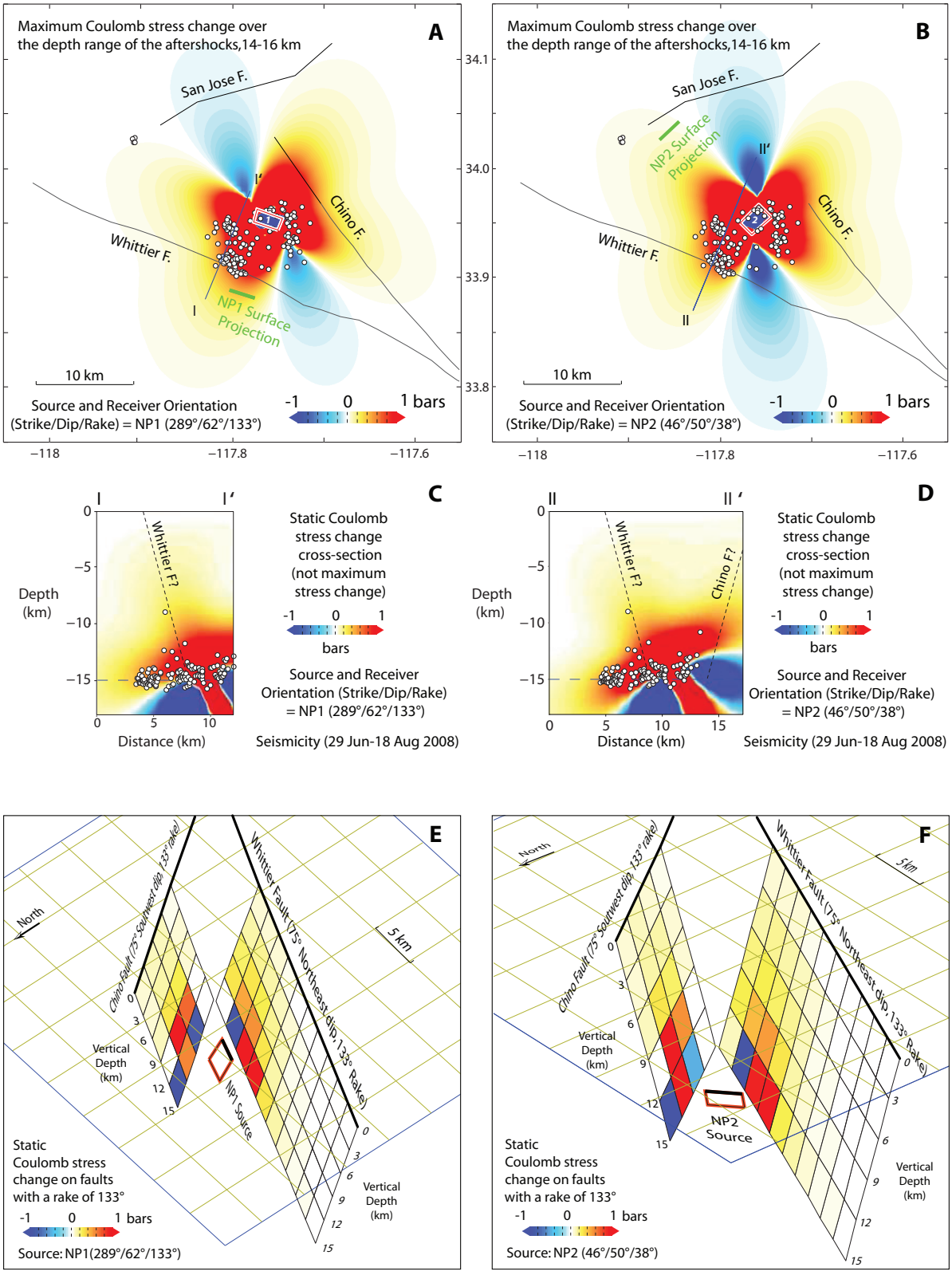

▲ **Figure 8.** (A–B) Maximum Coulomb stress change over the depth range of the aftershocks, using the two nodal plane solutions for both the source and receivers. Green lines indicate surface projection of the source to the ground surface, showing the mainshock nodal planes relative to the Whittier and San Jose faults. Black outlined white circles are aftershocks. (C–D) Static Coulomb stress change cross-sections with the aftershock plots; all aftershocks are projected onto the sections. (E–F) Static Coulomb stress changes resolved onto the Chino and Whittier faults by using their strike, a 75° dip, and 133° rake for the two candidate source faults, for nodal plane 1 and 2 sources. Black lines indicates top of the faults. All calculations using Coulomb 3.2 (http://www.coulombstress.org).

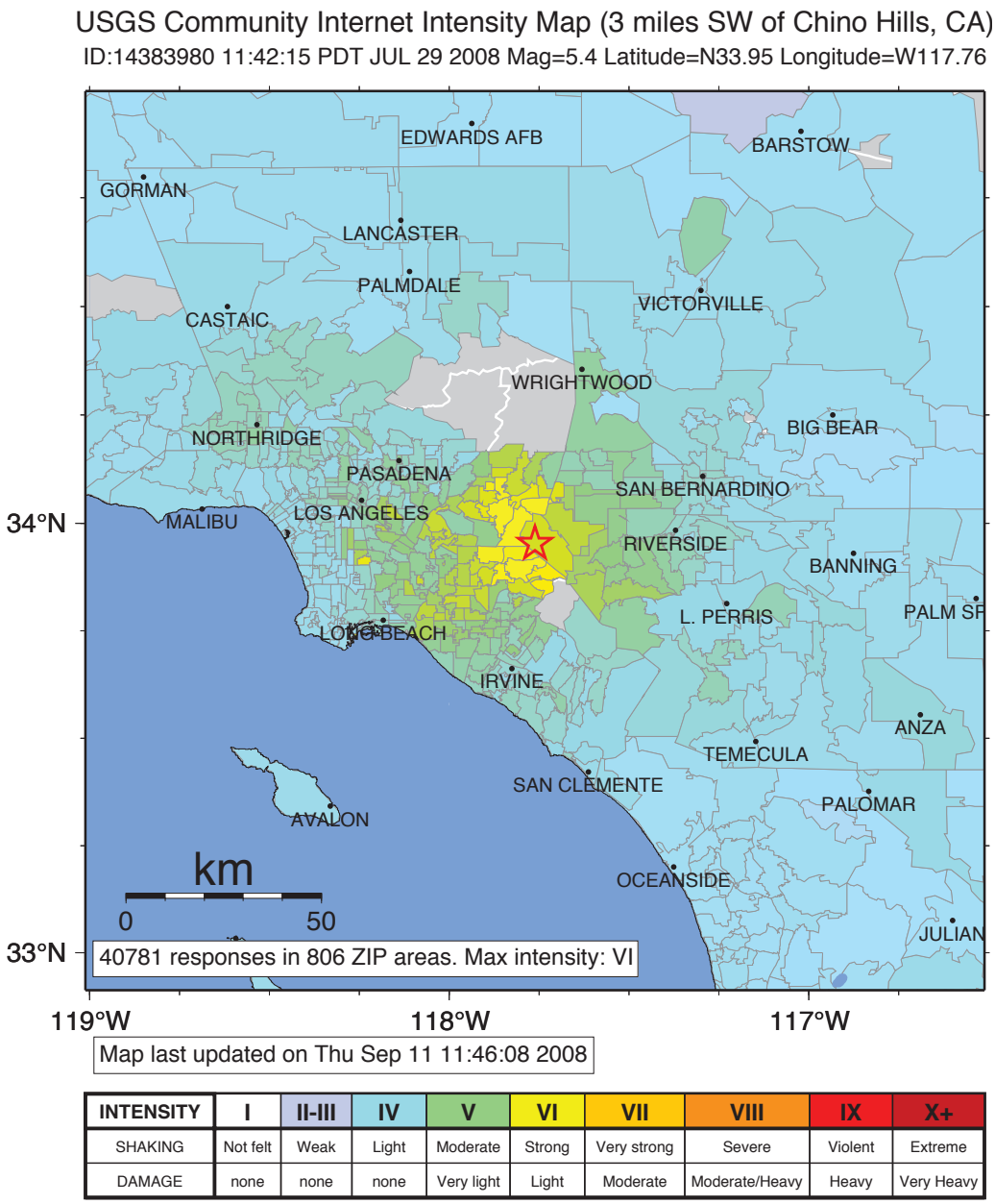

INTENSITY	I	II-III	IV	V	VI	VII	VIII	IX	X+
SHAKING	Not felt	Weak	Light	Moderate	Strong	Very strong	Severe	Violent	Extreme
DAMAGE	none	none	none	Very light	Light	Moderate	Moderate/Heavy	Heavy	Very Heavy

▲ **Figure 9.** "Did You Feel It?" community intensity map for the *Mw* 5.4 Chino Hills mainshock: http://pasadena.wr.usgs.gov/shake/ca/ (Wald, Quitoriano, Heaton *et al.* 1999).

sites where the maps do not agree, observed MMI values were lower than expectations, given instrumentally determined peak amplitudes. We suggest this might indicate that the relatively deep event generated less surface wave energy than a shallow event.

Both the ShakeMap (Figure 2) and the CIIM map (Figure 9) that are very well-constrained by data showing systematic variations that appear to correlate with near-surface geological structure. In particular, the 1- and 3-s spectral response ShakeMaps (see http://earthquake.usgs.gov/shakemap/),also capture the amplification at most of the hotspots in the CIIM map. To further explore the distribution of intensities in the CIIM data, we calculate the residuals by subtracting MMI_{pred} from Equation 2 at a given distance from the average MMI_{obs}, and compare the results to topography. To reduce scatter, we plot residuals at locations for which four or more reported MMI are available, resulting in a map of residuals with a range of ±1 unit (Figure 10A).

Focusing on the greater Los Angeles region, we tentatively identify a number of suggested systematic patterns in the distribution of intensities (Figure 10A). First, intensities are, as expected, generally lower at hard-rock sites, for example on the Palos Verdes Peninsula. Second, intensities are systematically higher in the deepest (central) Los Angeles basin, consistent with a basin-depth effect (*e.g.*, Joyner 2000). Third, intensities are systematically lower to the west of the Newport-Inglewood fault, a pattern that correlates with subtle topographic relief in proximity to the fault zone and the shallower basin depth

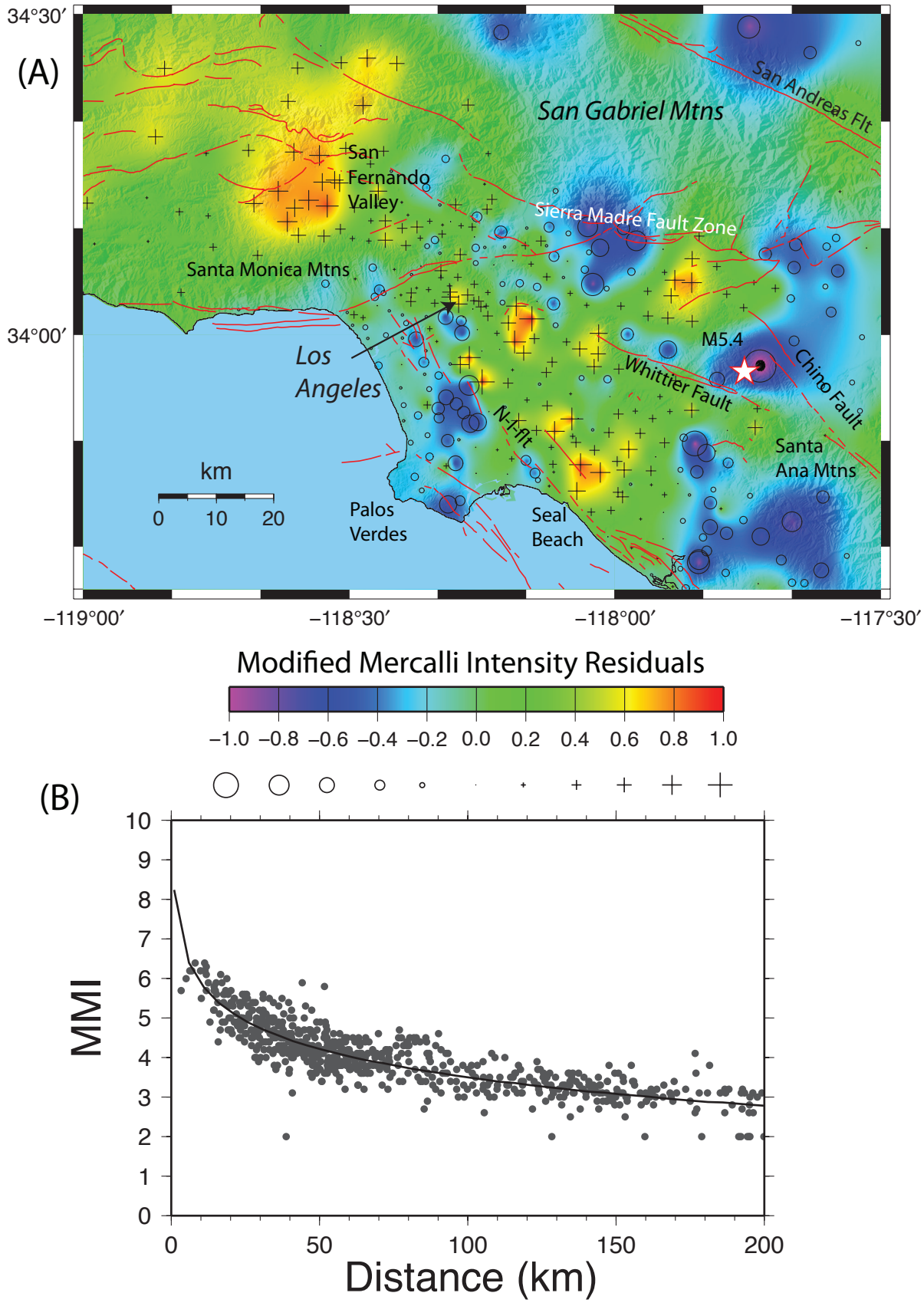

▲ **Figure 10.** (A) Map consisting of gridded MMI residuals, intensity residuals in the greater Los Angeles area on a topographic base for delineating the variations in local terrain. (B) The attenuation curve for MMI values from the data plotted in the "Did You Feel It?" map.

west of the fault. Fourth, there is a suggestion that intensities are systematically slightly higher at the western half of the San Fernando Valley, consistent with a shoaling effect at basin edges. Fifth, intensities are systematically higher to the north, northwest, and west, and lower toward the east even at sites in the San Bernardino basin where amplification is expected. These patterns are not easily explained by near-surface geology, and may reflect complex path and source effects.

DISCUSSION

Both north-south thrust and left-lateral faulting on the west-southwest striking faults accommodate ongoing north-south compression of the Transverse Ranges and the compression and lateral block movements within the Los Angeles basin to the south (Hauksson 1994). The moment tensor of the 2008 Chino Hills earthquake, which reveals oblique mixed thrust and left-lateral slip on an east-northeast or alternatively on a north-northwest-striking nodal plane, is consistent with previously proposed models of the Los Angeles basin tectonics. Such crustal deformation both accommodates crustal shortening as well as westward translation of crustal blocks within the Los Angeles basin (Hauksson 1994; Walls *et al.* 1998).

The unusual aspects of the sequence include a large difference between *ML* and *Mw*, low aftershock productivity, limited depth range of the subhorizontal aftershock distribution, and high mainshock stress drop. The mainshock appears to have left behind almost no residual stresses, thus causing only a few aftershocks near the mainshock fault plane. Most of the recorded aftershocks are in three off-fault clusters, suggesting static or dynamic triggering from the mainshock. The high stress drop in the mainshock suggests high stresses at depth, near the brittle ductile transition zone, consistent with previous studies (*e.g.*, Jones and Helmberger 1996). The discrepancy between *ML* and *Mw* is further consistent with expectations for a high stress-drop event. This, and other previous high stress-drop earthquakes that may be occurring within the northern edge of the Peninsular Ranges batholith, suggests possibly incipient faulting as the San Gabriel range front tectonic deformation migrates to the south.

Using detailed analysis of more than a decade of Global Positioning System (GPS) data, Argus *et al.* (2005) pointed out the discrepancy between the measured geodetic and geological fault slip rates in the northern Los Angeles basin. Because the geologically measured fault slip rates are significantly lower, there may be other crustal deformation processes accommodating the tectonic deformation. One possibility is aseismic slip along subhorizontal decollement surfaces (Fuis *et al.* 2001). However, there is no clear evidence for aseismic slip, either steady or episodic, along large decollement surfaces. In part, GPS data may not be sampled frequently enough or may not be sensitive enough to detect deep and low-amplitude slip events. Geodetic monitoring with higher sampling rates and sensitivity would be required to further explore the possibility that slow-slip decollement events are occurring.

CONCLUSIONS

Preliminary analysis suggests that the *Mw* 5.4 Chino Hills earthquake was a high stress-drop event, similar to other moderate earthquakes in the region in recent years. The low productivity and nearly complete absence of aftershocks in the vicinity of the mainshock hypocenter further suggests low residual stress near the mainshock rupture plane, which in turn suggests that the mainshock stress drop was nearly complete. However, the sparse aftershock distribution does not illuminate a rupture plane on the Whittier fault or any other mapped Late Quaternary fault in the area. The sequence occurred in the limited depth range of 13 to 16 km and thus provides new information about style of faulting and the state of stress just above the brittle-ductile transition zone. The observed intensity distribution further implies correlations between intensity/damage and mainshock depth or stress drop. The static Coulomb stress modeling, based on the moment tensor of the mainshock, suggests that the mainshock caused some loading on portions of the Whittier and Chino faults.

ACKNOWLEDGMENTS

This research was supported by USGS internal funds; also by Grant 08HQGR0030 to Caltech and by grants from the Southern California Earthquake Center (SCEC) to Caltech. SCEC is funded by National Science Foundation (NSF) Cooperative Agreement EAR-0529922 and USGS Cooperative Agreement 07HQAG0008. We thank the SCSN/SCEDC staff for ensuring timely delivery of high-quality data. We also thank R. Yeats, T. Bjorklund, G. Fuis, L. Jones, R. Stein, D. Helmberger, and T. Heaton for feedback and discussions; J. Hardebeck, E. Pounders, and D. Wald for reviews; and P. Shearer for making his plotting program available. Most figures were done using GMT software (Wessel and Smith 1991). SCEC contribution number 1221. Contribution number 10,008, Seismological Laboratory, Division of Geological and Planetary Sciences, California Institute of Technology, Pasadena.

REFERENCES

Argus, D. F., M. B. Heflin, G. Peltzer, F. Crampe, and F. H. Webb (2005). Interseismic strain accumulation and anthropogenic motion in metropolitan Los Angeles. *Journal of Geophysical Research* **110**, B04401, doi:10.1029/2003JB002934.

Astiz, L., P. M. Shearer, and D. C. Agnew (2000). Precise relocations and stress-change calculations for the Upland earthquake sequence in southern California. *Journal of Geophysical Research* **105**, 2,937–2,853.

Atkinson, G. M, and D. J. Wald (2006). "Did You Feel It?" intensity data: A surprisingly good measure of earthquake ground motion. *Seismological Research Letters* **78**, 362–368.

Bent, A. L., and D. V. Helmberger (1989). Source complexity of the October 1, 1987, Whittier Narrows earthquake. *Bulletin of the Seismological Society of America* **94**, 9,548–9,556.

Bjorklund, T., and K. Burke (2002). Four-dimensional analysis of the inversion of a half-graben to form the Whittier fold-fault system of the Los Angeles basin. *Journal of Structural Geology* 24 (9), 1,369–1,397.

Bjorklund, T., K. Burke, R. S. Yeats, and H. Zhou (2002). Miocene rifting in the Los Angeles basin: Evidence from the Puente Hills half-graben, volcanic rocks and *P*-wave tomography. *Geology* **30** (5), 447–450.

Clinton, J. F., E. Hauksson, and K. Solanki (2006). An evaluation of the SCSN moment tensor solutions: Robustness of the M_W magnitude scale, style of faulting, and automation of the method. *Bulletin of the Seismological Society of America* **96** (5); doi:10.1785/0120050241.

Cohn, S. N., T. L. Hong, and D. V. Helmberger (1982). The Oroville earthquakes: A study of source characteristics and site effects. *Journal of Geophysical Research* **87**, 4,585–4,594.

Dreger, D., and D. V. Helmberger (1991a). Complex faulting deduced from broadband modeling of the 28 February 1990 Upland earthquake (ML = 5.2). *Bulletin of the Seismological Society of America*. **81**, 1,129–1,144.

Dreger, D., and D. V. Helmberger (1991b). Source parameters of the Sierra Madre earthquake from regional and local body waves. *Geophysical Research Letters* **18**, 2,015–2,018.

Dreger, D. S., and D.V. Helmberger (1993). Determination of source parameters at regional distances with three-component sparse network data. *Journal of Geophysical Research* **98**, 8,107–8,125.

Felzer, K. R., R. E. Abercrombie, and G. Ekstrom (2003). Secondary aftershocks and their importance for aftershock prediction. *Bulletin of the Seismological Society of America* **93**, 1,433–1,448.

Felzer, K. F., and E. E. Brodsky (2006). Decay of aftershock density with distance indicates triggering by dynamic stress. *Nature* **441**, 735–738.

Fuis, G. S., T. Ryberg, N. J. Godfrey, D. A. Okaya, and J. M. Murphy (2001). Crustal structure and tectonics from the Los Angeles basin to the Mojave Desert, southern California. *Geology* **29** (1), 15–18; doi: 10.1130/0091-7613(2001)029<0015:CSATFT>2.0.CO;2.

Gutenberg, B., and C. F. Richter (1944). Frequency of earthquakes in California. *Bulletin of the Seismological Society of America* **4**, 185–188.

Hardebeck, J. L., and P. M. Shearer (2002). A New method for determining first-motion focal mechanisms. *Bulletin of the Seismological Society of America* **92**, 2,264–2,276.

Hauksson, E. (1990). Earthquakes, faulting and stress in the Los Angeles basin. *Journal of Geophysical Research* **95**, 15,365–15,394.

Hauksson, E. (1994). The 1991 Sierra Madre earthquake: Seismological and tectonic analysis. *Bulletin of the Seismological Society of America* **84**, 1,058–1,074.

Hauksson, E., and L. M. Jones (1991). The 1988 and 1990 Upland earthquakes: Left-lateral faulting adjacent to the central Transverse Ranges. *Journal of Geophysical Research* **96**, 8,143–8,165.

Hough, S. E. (2005). Remotely triggered earthquakes following moderate mainshocks (or, why California is not falling into the ocean). *Seismological Research Letters* **76**, 58–66.

Jennings, C. W. (1994). Fault activity map of California and adjacent areas: California Department of Conservation, Division of Mines and Geology, Geologic Data Map No. 6, scale 1:750,000.

Jones, L. E., and D. V. Helmberger (1996). Seismicity and stress drop in the eastern Transverse Ranges, southern California. *Geophysical Research Letters* **23**, 233–236.

Jones, L. M., K. E. Sieh, E. Hauksson, and L. K. Hutton (1990). The December 3, 1988 Pasadena, California earthquake: Evidence for strike-slip motion on the Raymond fault. *Bulletin of the Seismological Society of America* ***80***, 474–482.

Joyner, W. B. (2000). Strong motion from surface waves in deep sedimentary basins. *Bulletin of the Seismological Society of America* **90**, S95–S112.

Kanamori, H., and E. Brodsky (2004). The physics of earthquakes. *Reports on Progress in Physics* **67**, 1,429–1,496.

Kanamori, H., J. Mori, E. Hauksson, T. H. Heaton, L. K. Hutton, and L. M. Jones (1993). Determination of earthquake energy release and M_L using TERRAscope. *Bulletin of the Seismological Society of America* **83**, 330–346.

Kanamori, H., and L. Rivera (2008). Source inversion of W phase: Speeding up seismic tsunami warning. *Geophysical Journal International* **175** (1), 222–238.

Lin, J., and R. S. Stein (2004). Stress triggering in thrust and subduction earthquakes, and stress interaction between the southern San Andreas and nearby thrust and strike-slip faults. *Journal of Geophysical Research* **109**, B02303; doi:10.1029/2003JB002607.

Ludington, S., B. C. Moring, R. J. Miller, P. A. Stone, A. A. Bookstrom, D. R. Bedford, J. G. Evans, G. A. Haxel, C. J. Nutt, K. S. Flyn, and M. J. Hopkins (2007). *Preliminary Integrated Geologic Map Databases for the United States*, http://pubs.usgs.gov/of/2005/1305/.

Matthews, M.V., and P. A. Reasenberg (1988). Statistical methods for investigating quiescence and other temporal seismicity patterns. *Pure and Applied Geophysics* **126**, 357–372.

Reasenberg, P. A., and L. M. Jones, (1989). Earthquake hazard after a mainshock in California. *Science* **243**, 1,173–1,176.

Shaw, J. H., and P. M. Shearer (1999). An elusive blind-thrust fault beneath metropolitan Los Angeles. *Science* **283**, 1,516–1,518.

Shearer, P. M. (1997). Improving local earthquake locations using the L1-norm and waveform cross-correlation: Application to the Whittier Narrows, California, aftershock sequence. *Journal of Geophysical Research* **102**, 8,269–8,283.

Shearer, P. M., G. A. Prieto, and E. Hauksson (2006). Comprehensive analysis of earthquake source spectra in southern California. *Journal of Geophysical Research* **111**, B06303; doi:10.1029/ 2005JB003979.

Somerville, P. G., J. P. McLaren, L.V. LeFever, R. W. Burger, and D. V. Helmberger (1987). Comparison of source scaling relations of eastern and western North American earthquakes. *Bulletin of the Seismological Society of America* **77**, 322–346.

Toda, S., R. S. Stein, K. Richards-Dinger, and S. Bozkurt (2005). Forecasting the evolution of seismicity in southern California: Animations built on earthquake stress transfer. *Journal of Geophysical Research* B05S16; doi:10.1029/2004JB003415.

Utsu, T. (1961). A statistical study on the occurrence of aftershocks. *Geophysical Magazine* **30**, 521–605.

Wald, D. J., V. Quitoriano, L. Dengler, and J. W. Dewey (1999). Utilization of the Internet for rapid community intensity maps. *Seismological Research Letters* **70**, 680–697.

Wald, D. J., V. Quitoriano, T. H. Heaton, H. Kanamori, C. W. Scrivner, and C. B. Worden (1999). TriNet ShakeMaps: Rapid generation of peak ground motion and intensity maps for earthquakes in southern California. *Earthquake Spectra* **15** (3), 537–556.

Waldhauser, F., and W. L. Ellsworth (2000). A double-difference earthquake location algorithm: Method and application to the northern Hayward fault, California. *Bulletin of the Seismological Society of America* **90**, 1,353–1,368.

Walls, C., T. Rockwell, K. Mueller, Y. Bock, S. Williams, J. Pfanner, J. Dolan, and P. Fang (1998). Escape tectonics in the Los Angeles metropolitan region and implications for seismic risk. *Nature* **394**, 356–360.

Wessel, P., and W. H. F. Smith (1998). New version of the generic mapping tools released. *Eos, Transactions, American Geophysical Union* **79,** 579.

Zhao, L. S., and D. V. Helmberger (1994). Source estimation from broadband regional seismograms. *Bulletin of the Seismological Society of America* **84** (1), 91–104.

Zhu, L., and D. V. Helmberger (1996). Advancement in source estimation techniques using broadband regional seismograms. *Bulletin of the Seismological Society of America* **86** (5), 1,634–1,641.

Zhu, L., and L. A. Rivera (2002). A note on dynamic and static displacements from a point source in multilayered media. *Geophysical Journal International* **148**, 619–627.

California Institute of Technology,
Seismological Laboratory, MC 252-21
Pasadena, California 91125 U.S.A.
hauksson@gps.caltech.edu
(E.H.)